Geohazard Mechanics 1 (2023) 58–68

Contents lists available at ScienceDirect

Geohazard Mechanics

journal homepage: www.keaipublishing.com/en/journals/geohazard-mechanics

Quantitative assessment of energy changes in underground coal excavations using numerical approach

Chunchen Wei *, Chengguo Zhang, Onur Vardar, John Watson, Ismet Canbulat

School of Minerals and Energy Resources Engineering, University of New South Wales, Sydney, NSW, 2052, Australia

ARTICLE INFO

Keywords:
Coal burst
Energy changes
Numerical approaches

ABSTRACT

Coal burst is caused by a dynamic and unstable release of energy within the overstressed rock mass/coal during the mining process. Although the occurrence of coal burst is a result of the complex impacts of many factors, a major component of coal burst mechanism is associated with energy storage and release. This study reviewed the sources of energy that can contribute to a coal burst, principally strain and potential energy stored in the coal mass around excavations, and radiated seismic energy released by geological discontinuities. The energy balance concept proposed by [1] was utilised in numerical modellings to compute the radiated seismic energy in a modelling system and the kinetic energy of ejected rock/coal for a given burst scenario. The modelling results showed that the strain energy density (SED) around excavations increases with increasing mining depth and the maximum SED area migrates deeper into the coal. For the effect of geological features on both roadway and longwall face, the coal burst risk proneness can be assessed considering the proposed energy terms. According to the results of energy changes in excavations, the modelling predicts that for depths of ejection 2 m and 3 m the kinetic energy of a burst increases as the mining depth increases from 100 m to 1000 m, but for depth of ejection 1 m only increases until mining depth reaches 700 m and then decreases. The proposed energy-based model indicators can deepen the understanding of energy changes and the associated coal burst risks for different mining conditions.

1. Introduction

Coal burst is caused by a dynamic and unstable release of energy within the overstressed rock mass/coal during the mining process. Although the occurrence of coal burst is a result of the complex impacts of many factors [1–3], a major component of coal burst mechanism is associated with energy storage and release. The energy-based approach assesses the potential and intensity of coal bursts by evaluating the energy conversion process during underground excavations.

Cook is the pioneer of applying the energy approach to analyse the problem of rockburst in underground mines [4,5]. [5] pointed out that the damage produced by rockbursts was correlated to the excess potential energy generated by underground excavations. He adopted the elastic theory to quantitatively describe the deformation around underground excavations, showing that a large amount of gravitational potential energy converts to other forms of energy and at least half of the energy change is released in one form or another. The released energy is either in the form of non-violent dissipation or in the form of violent events. Thus, rockburst occurs when the energy release rate is greater than the rate at which energy can be dissipated non-violently during excavations, which forms the initial concept of Energy Release Rate (ERR) criterion. This criterion was then widely applied in underground mines in South Africa and it was found that the ERR value has a strong correlation with rockburst occurrence [6–10].

In the following years, researchers further studied the energy changes during mining and provided detailed calculations of the energy balance and the associated energy components [11–14]. For example [15], followed Cook's logic [5] and rigorously analysed the energy changes in the underground mining process. He stated that the excess energy can simply be described as the difference between the work done by the external forces and the total stored and dissipated energies, which is further discussed in Section 3. Furthermore, since ERR is limited for estimating the impacts of geological discontinuities [16], proposed the excess shear stress (ESS) criterion to specifically assess the possible seismic energy and seismic magnitude produced by fault-slip.

With improvements in computational power and advanced numerical modelling techniques in recent decades, the energy-based approach has been extended to use in a more realistic scenario: the excavations can be

* Corresponding author.
E-mail address: chunchen.wei@unsw.edu.au (C. Wei).

https://doi.org/10.1016/j.ghm.2022.11.003
Received 25 September 2022; Received in revised form 18 November 2022; Accepted 22 November 2022
Available online 26 November 2022

simulated within the rock mass that is allowed to have plastic deformations and fracture formation [17]. A number of researchers studied unstable failures and rockbursts using the energy calculations and advanced explicit numerical method software packages such as FLAC3D [18,19], 3DEC [20], UDEC [21–27], PFC [19] and Abaqus [28–31]. These studies once again demonstrated the robustness of the energy approach in evaluation of mining-induced seismicity and associated burst occurrences.

This study reviewed the sources of energy that can contribute to a coal burst and the energy balance of a mining cycle. Previous modelling studies conducted by the authors [17,32,33] have investigated the energy components associated with underground coal excavations in various geological conditions. This study summarised the previous modellings [17,32,33] to explore the capacities of numerical approaches in assessing the energy changes in development and longwall retreat. In addition, this study further estimated the kinetic energy of ejected material for given burst scenarios using the concept of energy balance, facilitating the quantitative assessment of coal burst risk proneness.

2. Assessment of energy components

In view of the energy considerations, there are various energy components. Gravitational potential energy depends upon the elevation of the rock or coal. Strain energy is the energy stored in rock and coal due to deformation, and the external work done on the rock and coal in causing it to distort from its unstressed state is usually transformed into strain energy. Another component, kinetic energy, is the energy possessed by coal in motion. This section discusses the numerical assessment approach of the energy components in underground excavations.

2.1. Strain energy

The strain energy stored in the rock units and coal is related to the stress and stiffness of the materials. The general equation of strain energy density, in J/m^3, within rock units is:

$$SED = \frac{1}{2E}\left[\left(\sigma_1^2+\sigma_2^2+\sigma_3^2\right) - 2\nu\left(\sigma_1\sigma_2+\sigma_1\sigma_3+\sigma_2\sigma_3\right)\right] \quad (1)$$

Where E is the Young's Modulus of rock units; ν is the Poisson's ratio; σ_1, σ_2, σ_3 are the principal stress components.

According to Equation (1), the pre-mining strain energy density within a coal seam at a given depth is approximated in Table 1, assuming Young's modulus of coal is 2 GPa, and Poisson's ratio is 0.25. The maximum horizontal stress (σ_1) is two times the vertical stress (σ_2), and the minimum horizontal stress (σ_3) equals the vertical stress. The SED increases exponentially with increasing cover depth.

2.2. Seismic energy

Fault-slip bursts, as the name implies, are caused by a sudden movement (*i.e.,* slip) along a geological fault which can generate seismic events with a Richter magnitude M_L of up to 5.0 [34–36]. The fundamental mechanics of these events are very similar to earthquakes, and their magnitudes are mainly controlled by the surface area of the discontinuity, the shear displacement distance and the stress drop magnitude. Once the slip is initiated, the peak frictional coefficient rapidly attains the lower residual frictional coefficient, resulting in excess energy being released and transmitted through rock mass as seismic waves [37]. At the instant, those shock waves encounter highly stressed rock, close to excavations, violent and dynamic rock failures may occur [38].

Table 1
Strain energy densities (SED) within coal seam at various depths [33].

Mining depth (m)	100	300	500	700	850	1000
SED (kJ/m^3)	5.5	49.2	136.7	268.0	395.1	546.9

Seismic source parameters are reliable and useful to measure fault-slip related seismic events [39,40]. Source parameters include stress drop $\Delta\tau$, seismic energy E_S, seismic moment M_o, and moment magnitude M. These parameters were introduced in a number of fundamental studies [41,42] and are widely used to evaluate the magnitude of earthquake and mining-induced seismicity [39,43–50]. Therefore, the explicit evaluation method is promising to quantitatively assess the mining-induced fault-slip behaviour with collaboration of advanced numerical techniques.

$$E_s = 0.5\Delta\tau\overline{D}A \quad (2)$$

Where $\overline{D}$ is the average shear displacement along the fault; A is the area where sliding takes place; $\Delta\tau$ represents the stress drop defined as the average difference between the shear stress on the fault before and after excavations. In numerical modelling, the parameters in Equation (2) can be explicitly computed during excavations, hence the quantitative assessment of the seismic energy released by fault-slip induced by mining.

Gas expansion energy is also an important energy component contributing to dynamic rock failures. In coal mining sector, the term outburst refers to coal ejection mainly driven by *in situ* gas pressure in the coal, whereas no or minimal gas pressure is involved in a coal burst event [51–53]. Thus, the assessment of gas expansion energy is not within the scope in this paper.

3. Numerical approach to assess energy changes in underground excavations

Section 2 discusses the assessment approach of individual energy components. However, these energy components do not take into account other energy terms within the system (*e.g.,* energy dissipation and plastic work done). In the concept of energy balance, as discussed in Introduction [15], investigated the energy changes in underground excavations. The study proposed that, before and after an excavation, the total released energy, W_r, can be expressed in the following two forms [15]:

$$W_r = U_m + W_k \quad (3)$$

$$W_r = (W + U_m) - \left(U_c + W_s + W_p + W_j\right) \quad (4)$$

Where U_m represents the strain energy stored within the mined-out portion of the rock mass whereas W_k is the total radiated seismic (i.e. kinetic) energy in which would be dissipated through damping until the new equilibrium is attained [15,54]. W denotes the work done by the external and body forces. Before and after one excavation, the change in the strain energy stored in the volume of rock that remains unmined is denoted by U_c. The dissipating energy expended through the loading and deforming of supports is denoted by W_s. Of note is that no support elements were considered in the numerical modellings in this study, hence $W_s = 0$. W_p and W_j represent the energy expended in plastic deformation of intact rock and frictional work done by pre-existing discontinuities, respectively.

In this study, static modelling mode was implemented for all models using the Universal Distinct Element Code (UDEC). Each of the energy terms in Equation (3) and Equation (4) can be explicitly calculated for an excavation scenario [55]. The energy terms are calculated using the same general nomenclature developed by Ref. [15] at every computing step and a running sum of each energy term is also recorded. In practice, the radiated seismic energy component (W_k) can be recorded by mine microseismic systems, and is the controlling factor for the damage caused by a rockburst [12,34,54,56,57]. Furthermore, for a given rock/coal burst scenario, the total released energy (W_r) before and after the burst can be approximately regarded as the kinetic energy of the ejected material.

4. Quantification of energy changes and discussion

4.1. Assessment of strain energy in roadway development and longwall

In this section, a previous modelling conducted by the authors [33] is used to demonstrate the quantification of the strain energy stored within the rock mass surrounding excavations using the Universal Distinct Element Code (UDEC). A comprehensive parametric numerical analysis is carried out to assess the role of the contributing factors in development roadway and longwall face. The material properties, constitutive models and other modelling information were discussed in detail in the previous study [33]. The model configuration and boundary conditions are shown in Fig. 1.

The mining height was 3 m for both the longwall and development models. Six mining depths ranging from 100 m to 1000 m were conducted in the modelling. The vertical load determined by the depth of mining was applied at the top of the modellings, while the maximum and minimum horizontal stresses were two and one times the vertical stress, respectively. In the longwall model, the panel is excavated for a distance of 400 m. The mining depth increased from 100 m to 1000 m. The strain energy density (SED) ahead of the longwall face is calculated at the end of the longwall retreat for each mining depth. An example of SED contour around longwall and roadway development is shown in Fig. 2. The SED was computed using Equation (1) for coal seam in the modelling during excavations. Then, the maximum value of SED was picked up and the corresponding position of the maximum SED point can be identified. The

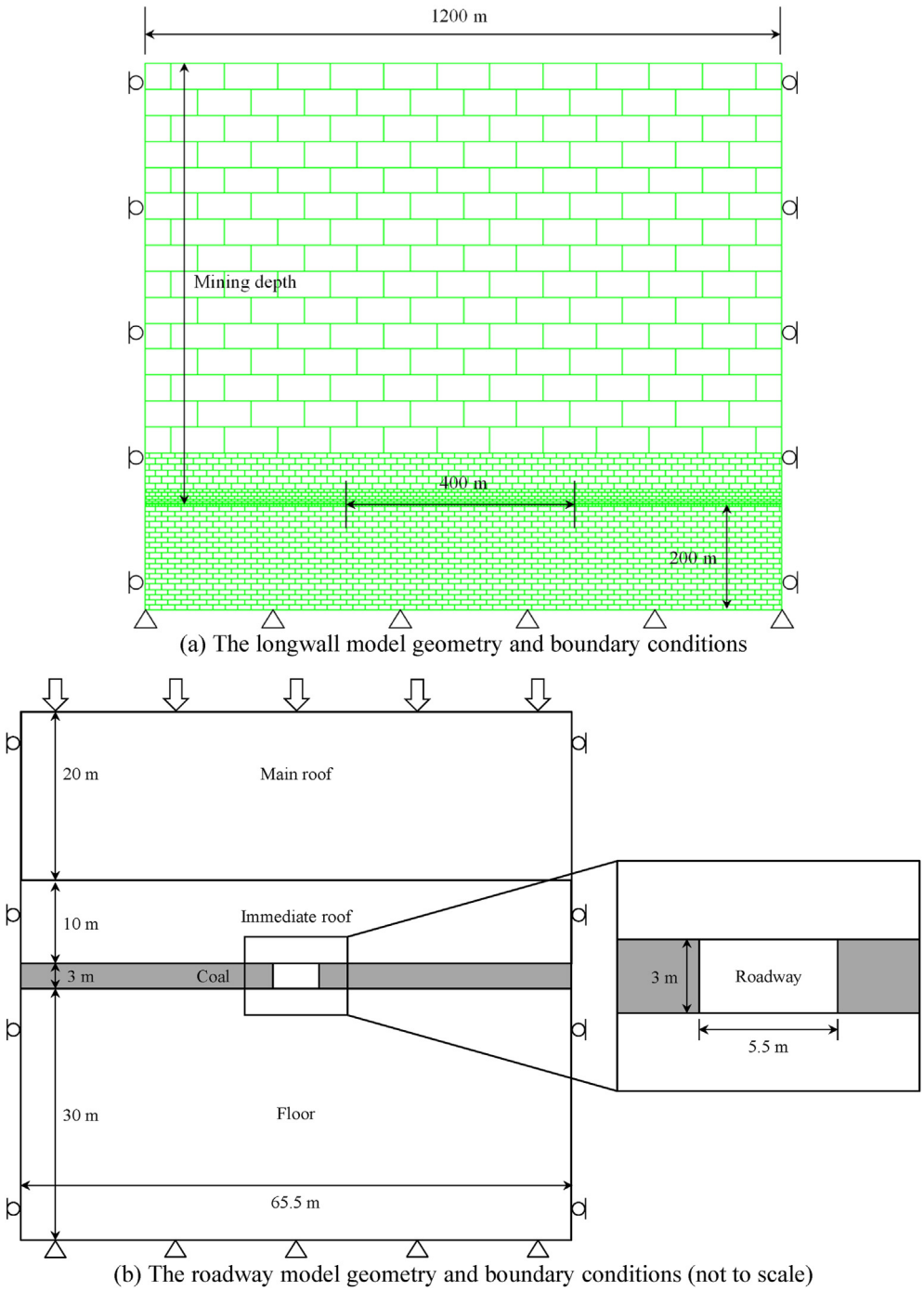

Fig. 1. Model configuration and boundary conditions [33].

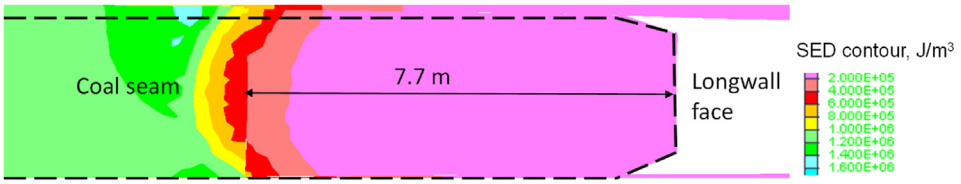

(a) An example of strain energy density contours in the coal seam at the longwall face for 700m mining depth (with deformable mesh)

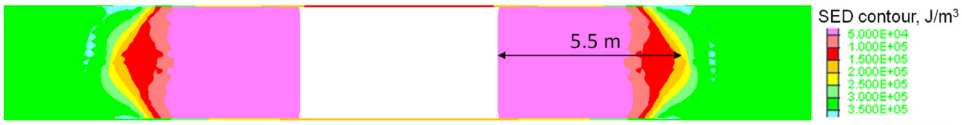

(b) An example of energy density contours in the coal seam at the ribs for development at 700m mining depth

Fig. 2. Examples of SED contours in numerical modellings [33].

coal mass between the maximum SED point and the longwall face is generally in a yielded state, in which the SED is less than that stored in the coal seam before mining (i.e., *in situ* state). For both longwall and development models the blocks are deformable and the zone size within blocks is 0.5 m by 0.5 m in the coal seam, increasing gradually through the rock to the outer boundaries. As shown in Fig. 3, the maximum SED area migrates outbye the longwall face with increasing mining depth. The distance increases drastically from 3 m to 6 m when the mining depth increases from 100 m to 300 m. Then it increases slowly up to 8 m at 1000 m mining depth.

In Fig. 4, the maximum SED in the longwall outby the yielded coal mass is summarised for various mining depths. Fig. 4 also compares the maximum SED to that of the coal seam in the *in situ* stress state, of which values are listed in Table 1. As expected, the strain energy stored in the coal seam increases significantly following the introduction of longwall excavation. At shallower depth, even though the increase in maximum SED is substantially higher than the deeper depths (*e.g.*, the difference of 2000% at 100 m versus 310% at 1000 m), the final magnitudes are significantly higher at greater depths. This means that the magnitude of the strain energy stored around the excavation increases with increasing mining depth. The maximum SED is approximately 1710 kJ/m^3 outbye the longwall face when the mining depth is at 1000 m.

Similarly, the maximum SED and position relative to a roadway excavation are summarised in Figs. 5 and 6. As shown in Fig. 5, with increasing mining depth, the position of maximum SED has the same increasing trend as at a longwall face. The distance increases almost linearly from 0.1 m to 7.6 m when the mining depth increases from 100 m to 1000 m.

Similarly, the difference between the SED after introduction of the roadway in the model and the SED at pre-mining state increases with increasing mining depth. The magnitude of the maximum SED increases from approximately 6 kJ/m^3 to 780 kJ/m^3 when the mining depth

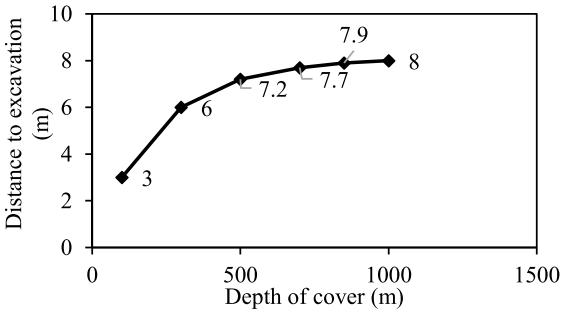

Fig. 3. The position of maximum SED area ahead of LW face [33].

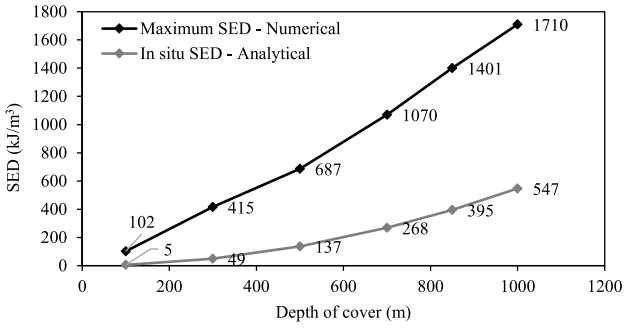

Fig. 4. The maximum SED at various mining depths ahead of LW face [33].

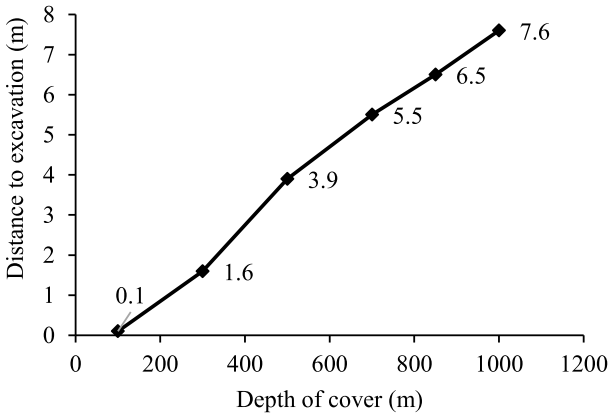

Fig. 5. The position of maximum SED at ribs for development roadway [33].

increases from 100 m to 1000 m. It is of note that the maximum SED around roadway ribs is smaller than that around a LW face at the same mining depth. This is because of the abutment load redistributions in longwalls. The pre-mining SED was computed using analytical solutions by Equation (1), while the after-mining SED was obtained through numerical modelling. Thus, a slight difference caused by the two different calculating scenarios exists in the SED values, which can be reflected in the SED comparisons in the shallower depth of mining (*e.g.*, 100 m and 300 m).

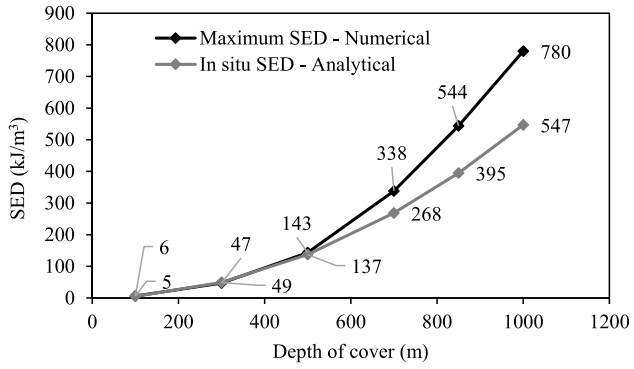

Fig. 6. The maximum SED at various mining depths at ribs for development [33].

4.2. Assessment of energy in geological features intersected by roadway excavation

This section investigates the impacts of geological faults on coal burst proneness by presenting the previous modelling outcomes developed by the authors [32]. The study incorporates the general geological and geotechnical environments of a roadway in an underground coal mine. The details of the modelling can be found in the previous study [32].

The fault plane is modelled on the right-hand side of the roadway and its minimum proximity to the roadway *d* and dip angle *a* are systematically varied during the parametric analysis. The model geometry, geological units and boundary conditions are illustrated in Fig. 7. The fault throw was assumed to be zero in the modelling as most of the normal faults in the mine site had a fault elevation difference of no more than 0.3 m. Furthermore, according to the conventional stress regime around normal faults [37], the ratios of maximum and minimum horizontal stresses to vertical stress were set to be 0.75 and 0.5, respectively, in the modelling [32]. The zone size was 0.25 m in coal and 1 m in roof and floor. The peak and residual friction angle was 25° and 10°, respectively, for the fault plane. The cohesion and tension were assumed to be zero along the fault, where the normal and shear stiffness was 50 GPa/m and 5 GPa/m, respectively.

The static equilibrium state was achieved using a mechanical damping scheme. Damping forces were applied at each timestep until attaining an equilibrium state after excavation. During the damping process, a fraction of kinetic energy generated within the system can be recorded in the numerical model. Hence, the total damping work during the excavation is regarded as the total radiated seismic energy [32,55]. The calculated radiated seismic energy values (W_k) during roadway excavation are used to assess the damage that can be caused by a potential coal burst [54]. In addition to the radiated seismic energy, the greatest kinetic energy recorded in any analysis is also considered as a key indicator of unstable failures and the rapidity of energy release [21,28,32].

To investigate the influence of fault proximity on roadway stability and energy release, a systematic and rigorous sensitivity analysis is conducted. A fault plane dipping at 75° is gradually brought closer to the roadway until it intersects the excavation (proximity = zero). A mining depth of 500 m is chosen as the Australian coal mine considered in the numerical modelling plans to operate at that depth in the future. After each increment of roadway excavation, the radiated seismic energy and peak kinetic energy values are computed. The results show that between the proximities of 10 m–20 m, no significant influence of the fault is observed, as shown in Fig. 8. As the distance between the fault and roadway is less than 10 m, it becomes active and the energy magnitudes firmly increase. This steady increase continues up to 6 m fault proximity where the highest seismic and peak kinetic energy magnitudes throughout the sensitivity study are computed: 2.31 MJ and 61.3 kJ per metre of roadway, respectively. When the fault is located less than 6 m from the roadway, the energy magnitudes start to decline, indicating that 6 m is the critical distance (critical fault proximity) for the given conditions where the influence of the fault is the greatest [32].

4.3. Assessment of energy in geological features during longwall retreat

This section presented the previous modellings conducted by the authors [17] to investigate the impacts of major fault on longwall retreat. The numerical model was based on the geological and geotechnical conditions in a mine site, as shown in Fig. 9. The zone size was 0.5 m by 1 m in the mining direction and its perpendicular direction (i.e., the

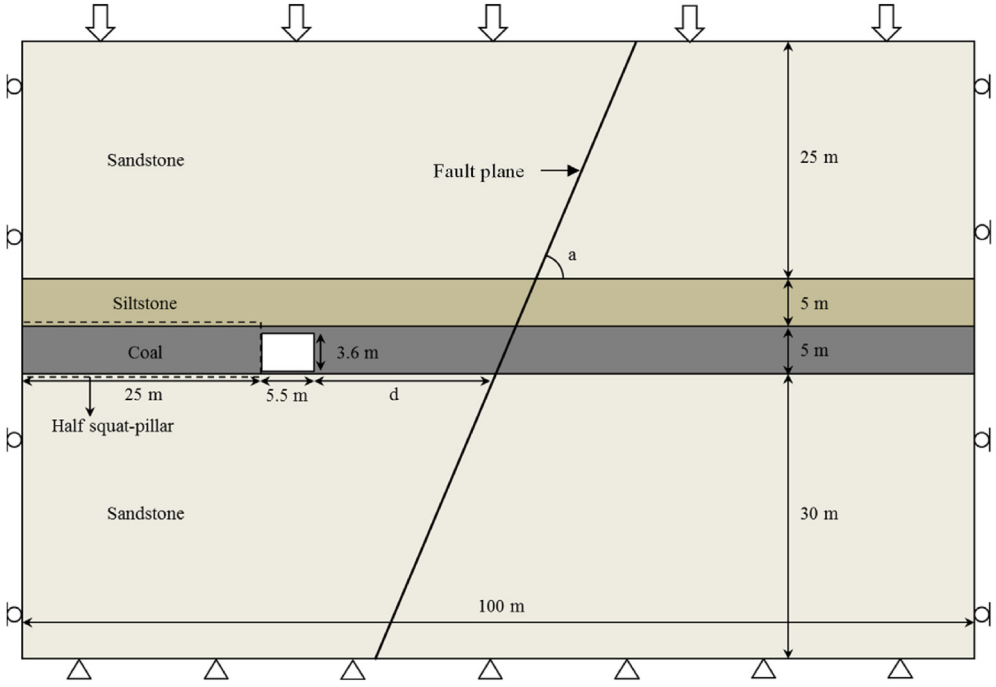

Fig. 7. Model geometry, geological units and boundary conditions [32].

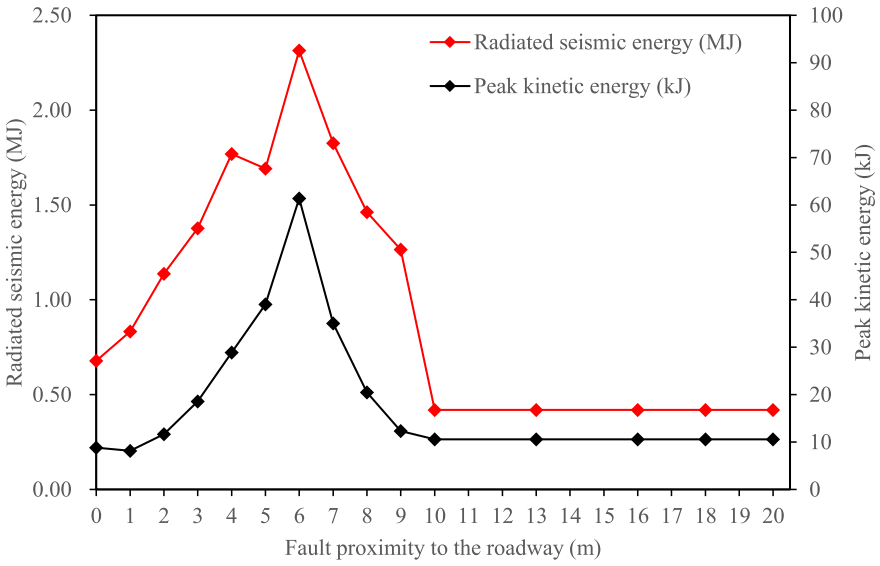

Fig. 8. Influence of fault proximity to the roadway on radiated seismic energy and peak kinetic energy [32].

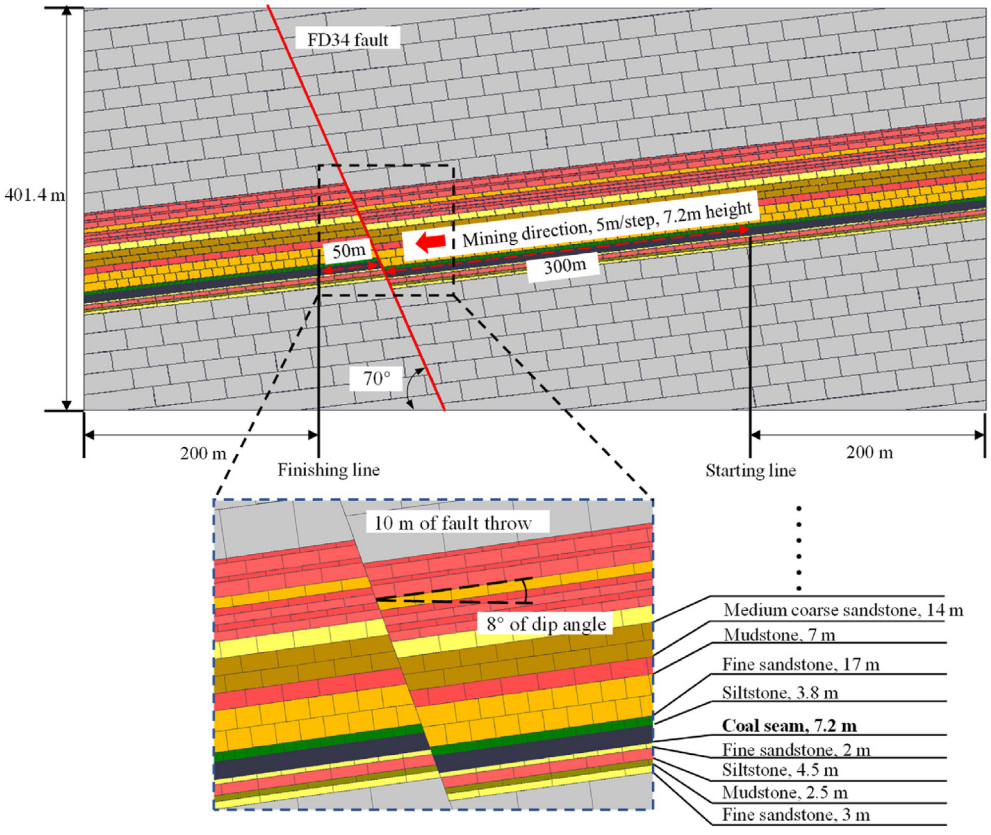

Fig. 9. Longwall model configuration [17].

inclined vertical direction), respectively. The zone size gradually increased from the coal seam to roof and floor. A vertical load determined by the depth of mining (850 m in this case study) was implemented on the top of the boundary. According to the field measurements of the *in situ* stress, the maximum (perpendicular to the longwall face) and minimum (out-of-plane direction) horizontal stresses were 1.4 and 0.85 times the vertical stress in the modelling. Based on a back analysis of the field observations of the microseismic energy, the peak and residual friction angle of the fault plane was determined to be 30° and 25°, respectively, and the cohesion and tensile strength were zero.

The radiated seismic energy (W_k, which is the model seismic energy in Fig. 10) of the model was calibrated against the change pattern of seismic energy observed in the mine site when the longwall face passed through the FD34 fault, as shown in Fig. 10. The fault seismic energy shown in Fig. 10 (b) is computed using Equation (2). Two other model indicators were also computed during the longwall excavations:

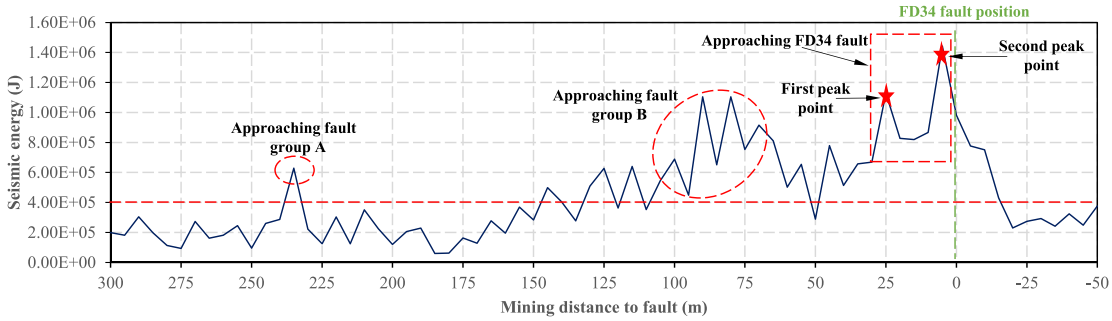

(a) Seismic energy recorded by the microseismic monitoring system during longwall retreat

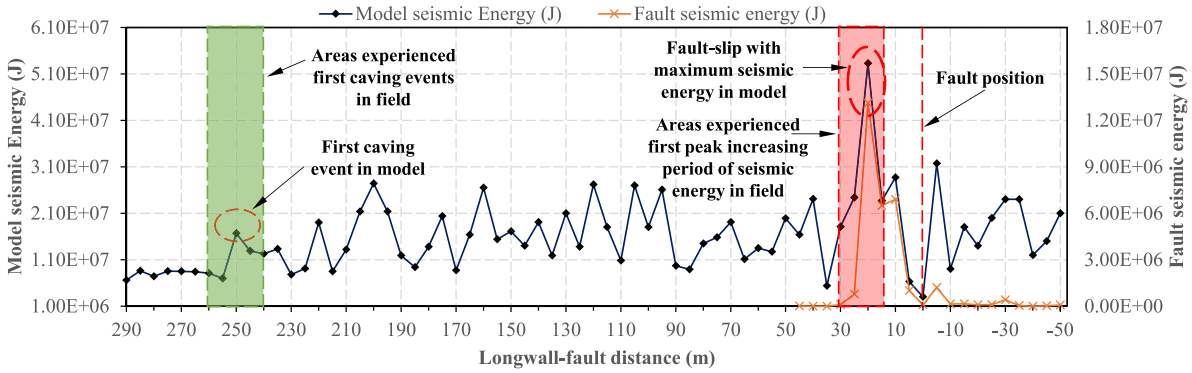

(b) Computed seismic energy released by longwall model

Fig. 10. Seismic energy observed in practice and computed in longwall model during progressive mining [17].

abutment stress and SED outbye the longwall face. The coal burst risk proneness of the longwall face can then be assessed by analysing the proposed energy-based model indicators [17].

The model was also validated by comparing the first caving distance observed in practice. The magnitude of model seismic energy remained below 9 × 10^6 J until the occurrence of the first caving event, which occurred at 250 m of longwall-fault distance (50 m of longwall excavation length). The first caving event rapidly released 1.67 × 10^7 J of seismic energy (see Fig. 11). In the field, the observed roof first caving distance (the span of the first weighting event) was approximately 40 m–60 m. It indicates that the first caving distance in the longwall model has a good agreement with that observed in the mine [17].

The change pattern of the model seismic energy was highly related to the development of the plastic area around excavations and the progressive caving events during the longwall mining [17]. The model seismic energy increased significantly from 2.44 × 10^7 J at 25 m of longwall-fault distance to 5.33 × 10^7 J at 20 m of longwall-fault distance, where the fault-slip event with the maximum released seismic energy occurred. Also, the seismic energy observed in practice experienced an increasing peak period when the longwall face approached FD34 fault from approximately 30 m–20 m of longwall-fault distance. The magnitude of 5.33 × 10^7 J was the largest amount of model seismic energy during the whole excavations. The model seismic energy then remained at relatively high magnitudes of 2.37 × 10^7 J and 2.87 × 10^7 J at 15 m and 10 m of longwall-fault distance, respectively. When the longwall face was close to the fault, the model seismic energy dropped to 6.30 × 10^6 J and 3.00 × 10^6 J at 5 m and 0 m of longwall-fault distance, respectively. Hence, the magnitude of model seismic energy was relatively higher when the longwall face approached the fault from 25 m to 10 m of longwall-fault distance. This was consistent with the change pattern of seismic energy monitored in practice, where large magnitudes of seismic energy were observed when the longwall-fault distance was from approximately 25 m–5 m [17].

When the longwall face approached close to the fault, both the peak abutment stress and maximum SED experienced a drastic increase from 45 m to 25 m of longwall-fault distance [17]. The peak abutment stress increased from approximately 45 MPa–53.4 MPa (8.4 MPa of increase). Additionally, the magnitude of 53.4 MPa was the maximum value of peak abutment stress before the longwall face passed the fault. The maximum SED increased from approximately 4.35 × 10^5J/m^3 at 45 m of longwall-fault distance to 5.30 × 10^5J/m^3 at 30 m of longwall fault distance and then slightly decreased to 5.03 × 10^5J/m^3 at 25 m of longwall-fault distance. After the drastic increase, both the peak abutment stress and maximum SED experienced a most significant drop from 25 m to 20 m of longwall-fault distance, where the fault-slip event with maximum released seismic energy occurred. The peak abutment stress decreased from 53.4 MPa to 35.7 MPa (17.7 MPa of abutment stress drop), and maximum SED dropped from 5.03 × 10^5 J to 2.74 × 10^5J/m^3 (2.29 × 10^5J/m^3 of SED drop). After the longwall face passed the fault, the peak abutment stress went back to a high magnitude between approximately 50 MPa and 58 MPa. The maximum SED also remained at a relatively high magnitude of between 5 × 10^5J/m^3 and 6 × 10^5J/m^3 [17].

Using the results from the field-calibrated model, a coal burst risk classification was developed when the longwall retreat approached and finally passed the FD34 fault [17]. The coal burst risk was classified into three levels: low-risk, medium-risk and high-risk, as shown in Fig. 12. The risk classification is determined based on the model results discussed above, including the magnitude of radiated seismic energy (i.e., W_k, the model seismic energy), and the magnitude and the positions of both the peak abutment stress and the maximum SED. It postulates that the coal burst risk increases with the increase of seismic energy magnitude, the increase of magnitude of the peak abutment stress and the maximum SED, the decrease of the distance between the two model indicators (peak abutment stress and maximum SED) and the longwall face [17]. Fig. 12 does not include the seismic energy released by fault-slip, as it has the

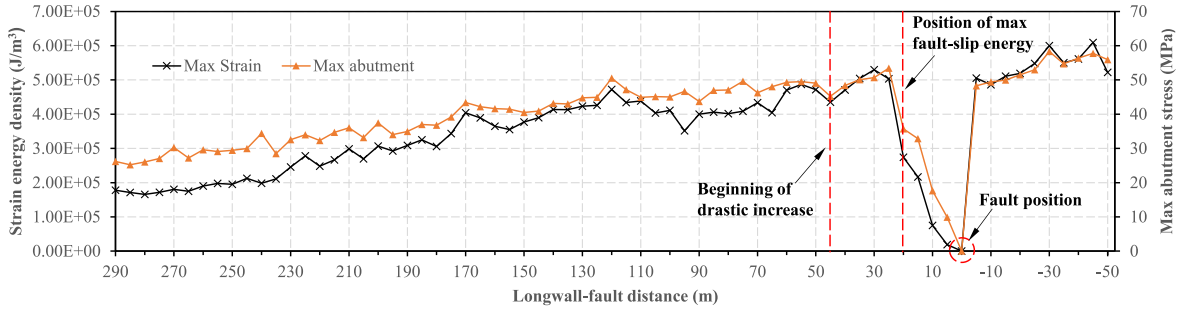

(a) Magnitude of peak abutment stress and maximum SED

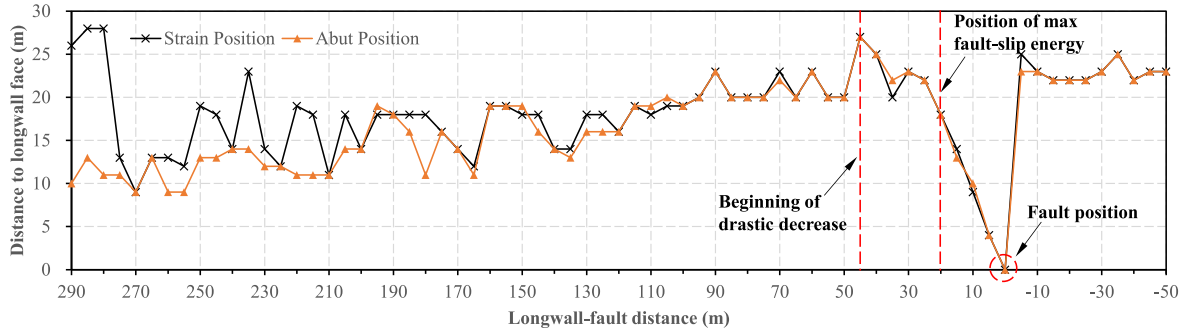

(b) Positions of peak abutment stress and maximum SED during longwall mining

Fig. 11. Peak abutment stress and maximum SED during longwall mining [17].

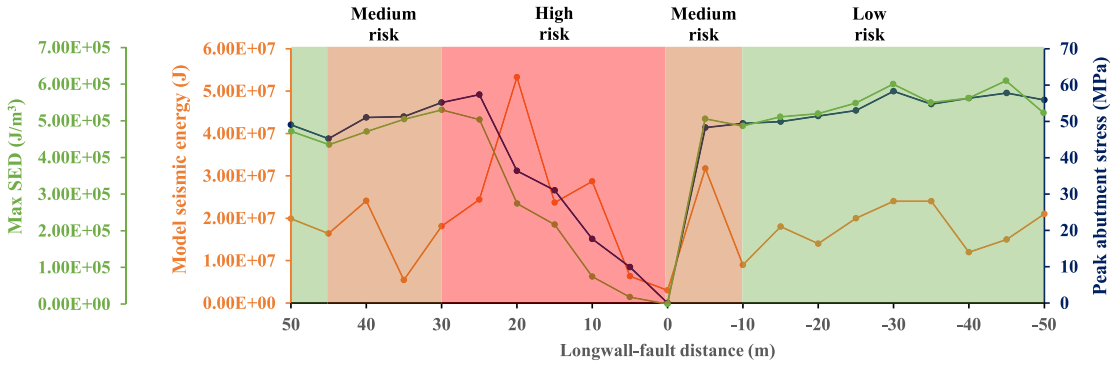

Fig. 12. Coal burst risk classification according to the model indicators [17].

same change pattern as that of the model seismic energy.

From 45 m of longwall-fault distance, the longwall mining went into a medium-risk zone, as the peak abutment stress and the max SED went into a strong increasing period and the fault-slip events began to generate seismic energy [17]. From 30 m to 0 m of longwall-fault distance, the longwall mining went into a high-risk zone. Both the peak abutment stress and the maximum SED increased to approximately the highest magnitude and their position started to move closer to the longwall face than before when the longwall face advanced from 30 m to 25 m of longwall-fault distance. From 25 m to 20 m of longwall-fault distance, shear displacement increased most drastically, and it generated the largest magnitude of seismic energy. From 20 m to 10 m of longwall distance, the seismic energy produced by both the fault-slip and the model remained at a relatively high level of magnitude. The position of peak abutment stress and maximum SED moved closer to the excavation boundary (approximately from 22 m to 9 m distant from the longwall face), although their magnitude reduced, as shown in Fig. 12. From 10 m to 0 m of longwall-fault distance, the coal seam at the hanging wall side was all in the plastic state, indicating that low levels of strain energy were stored within the coal mass. However, a large amount of strain energy was still stored within the rock mass at the footwall side that was next to the plastic coal seam. The highly stressed rock mass behind the plastic coal was at a critical state, which had the potential to generate a strain burst with minimal trigger energy. The distance between the high strain energy zone and the plastic coal mass decreased when the longwall face approached close to the fault. Furthermore, the trigger energy was at a relatively high level from 10 m to 0 m of longwall-fault distance [17].

The mining period from 0 m to -10 m of longwall-fault distance was

classified as a medium-risk zone. For the first excavation step after passing the fault (from 0 m to -5 m of longwall-fault distance), the magnitudes of fault seismic energy (1.20×10^6 J) and model seismic energy (3.18×10^7 J) were relatively higher than those released after [17].

After the longwall face passed within 10 m from the fault, the longwall mining went into a low coal burst risk area. The model seismic energy reduced to relatively low magnitudes and the magnitude of fault seismic energy was negligible. The peak abutment stress and maximum SED moved much deeper (approximately 22 m–25 m) into the longwall face than the situation before passing the fault, although their magnitude stayed high (after passing the fault) [17].

4.4. Assessment of the kinetic energy of ejected coal in roadway development and longwall

In this section, a coal burst scenario was examined for both development and longwall. The model configurations, material properties, and boundary conditions remain the same as Section 4.1. As shown in Fig. 13, the coal seam at the excavation boundary is further excavated into the rib by 1 m, 2 m and 3 m respectively to simulate a coal burst event with 1 m, 2 m and 3 m of ejection depth. Then, the kinetic energy (i.e., W_r) can be explicitly computed in the modelling for the ejected coal using Equation (4). For the longwall model, this section mainly focuses on the energy changes at the longwall face area after the burst event. In order to minimise the effect of energy induced from roof caving, the dense joints and beddings within roof and floor were not represented in this analysis. The excavation length is 12 m per step, and the total retreat length 240 m. During longwall retreat, the excavated coal is backfilled with an elastic material (500 MPa Young's modulus and 0.25 Poisson's ratio) to simulate the goaf consolidation [50].

According to Equation (4), the computed values of kinetic energy of ejected coal per metre of roadway and metre of longwall face are summarised in Figs. 14 and 15, respectively. As shown in Fig. 14, for the development scenario, both mining depth and ejection depth impact the kinetic energy of the ejected coal. When the depth of ejected coal is 1 m, the kinetic energy increases slightly when the mining depth increases from 100 m to 700 m. The kinetic energy then reduces marginally from 63 kJ to 57 kJ when mining depth increases from 700 m to 1000 m. In comparison, when the depth of ejected coal is 3 m, the kinetic energy increases markedly from approximately 22 kJ–1125 kJ when the mining depth increases from 100 m to 1000 m. Thus, when mining depth goes deeper, the associated kinetic energy increases significantly with increasing ejection depth.

As shown in Fig. 15, the changing pattern of kinetic energy in longwall retreat is similar to that in development. However, the magnitude of kinetic energy around the longwall face area is greater than that in the corresponding development scenarios. As shown in Fig. 15, the kinetic energy around the longwall face area increases drastically with increasing ejection depth when the mining depth increases. Similar to the development scenario, for 1 m burst cases, the kinetic energy increases when mining depth increases from 100 m to 700 m. Then, it decreases from 136 kJ to 3 kJ when mining depth increases from 700 m to 1000 m. This is mainly because the 1 m thick coal at the face is totally yielded when mining depth increases to 850 m and 1000 m, resulting in a minimal amount of kinetic energy released when coal burst occurs at such an ejection depth (*i.e.*, 1 m). However, when ejection depth increases to 2 m and 3 m, the kinetic energy increases with increasing mining depth. Furthermore, the increasing pattern of kinetic energy accelerates when mining depth increases from 500 m to 1000 m with the ejection depths of 2 m and 3 m.

In the above discussion, since the proposed method of analysis applies to all cases, the ejection of coal however caused is referred to as a coal burst. The prediction of whether or not a burst will occur in a given situation is a difficult task. The more modest aim of the work presented here is to predict, for a given mine layout and geological setting, whether a coal burst would be of unacceptable intensity were it to occur.

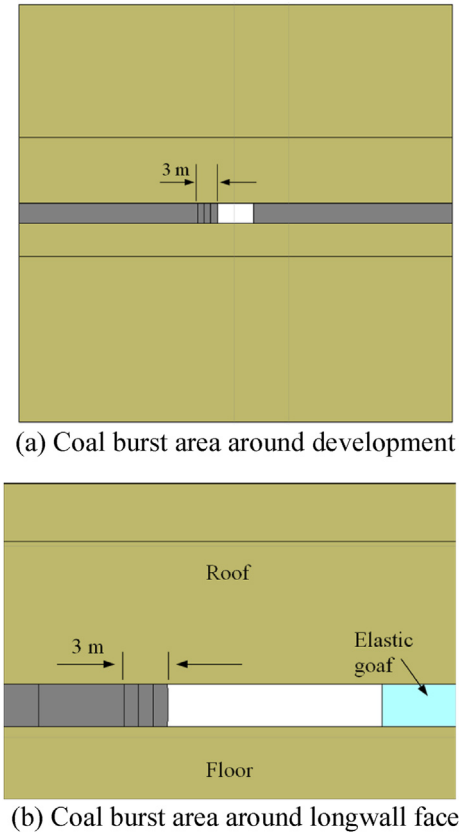

Fig. 13. Coal burst area around excavations.

4.5. Discussion

The purpose of the analyses shown in this study is to demonstrate the computation of energy terms in the vicinity of longwalls and roadways, to facilitate for example the prediction of bursts. Generalised input parameters are used in the modelling studies to understand those energy components. However, in principle, the analyses demonstrated here must be undertaken on a case by case basis, taking account of factors such as faults, mining configurations, roof and floor geology and the presence of pre-existing mine workings adjacent to or on different levels to the excavation under consideration. It may prove feasible to catalogue computed results for a small number of standard cases, but otherwise

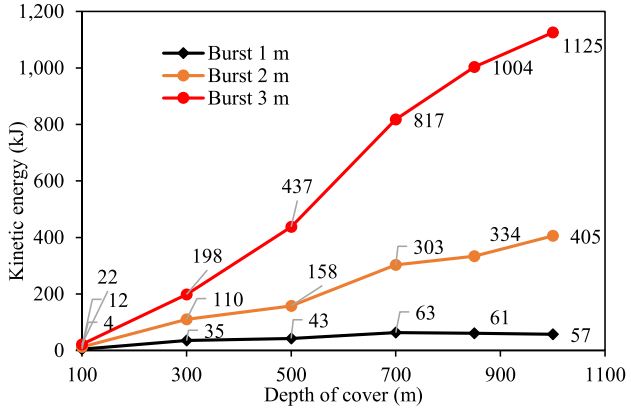

Fig. 14. Kinetic energy of ejected coal with various ejection depths per metre of roadway.

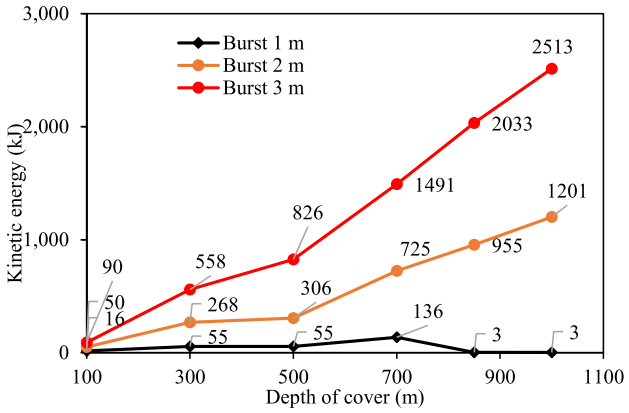

Fig. 15. Kinetic energy of ejected coal per metre of longwall face.

detailed numerical modelling studies are required. The correlation between the field measurements and the model indicators also needs further investigation.

Ejection velocities could be estimated from computed strain energy densities in the coal to be ejected, or more accurately from kinetic energies given by Equation (4) which are computed according to the equation of conservation of energy for the process of excavation of coal from the longwall.

5. Conclusion

In this study, the coal burst related energy sources are identified and calculated using numerical approach. The energy sources are categorised into strain and potential energy stored in the coal mass around excavations, and radiated seismic energy released by geological discontinuities. This study uses computer codes to undertake this work and define the energy sources in various locations such as mine roadways, longwall retreat, and geological structures. The gas expansion energy, as the main energy sources in outbursts, is however not considered in this study.

For development ribs and longwall face, the strain energy density (SED) increases with increasing mining depth and the maximum SED area migrates deeper into the coal. The maximum SED around roadway ribs is smaller than that around a longwall face at the same mining depth.

For the effect of a fault close to the roadway, the model results show that the energy release terms (radiated seismic energy and kinetic energy) are at their highest level when the fault proximity is 6 m. When the longwall face approached close to a major fault, a large amount of seismic energy can be released by the fault-slip. The largest fault-slip event occurred when the peak abutment stress and maximum SED in front of the longwall face experienced a most significant reduction. The coal burst risk proneness can be assessed using the proposed energy terms in the modelling.

According to the results of energy changes in excavations, the modelling predicts that for depths of ejection 2 m and 3 m the kinetic energy of a burst increases as the mining depth increases from 100 m to 1000 m, but for depth of ejection 1 m only increases until mining depth reaches 700 m and then decreases. For the worst scenario in this study (i.e., 3 m of burst thickness in 1000 m of depth of mining), the kinetic energy of ejected coal is approximately 2513 kJ and 1125 kJ, respectively, for longwall face and development.

The study showed that the energy-based model indicators can help to assess the coal burst risk proneness within various geological and mining domains. Also, the computed energy-term results can provide quantitative insights into coal burst control measures.

Funder

Australian Coal Industry's Research Program.Grant/Project Number: C26066.

Declaration of competing interest

The authors declare that they have no known competing financial interests or personal relationships that could have appeared to influence the work reported in this paper.

References

[1] A. Iannacchione, S.C. Tadolini, Occurrence, prediction, and control of coal burst events in the US, Int. J. Min. Sci. Technol. 26 (1) (2016a) 39–46.
[2] C. Zhang, I. Canbulat, B. Hebblewhite, C.R. Ward, Assessing coal burst phenomena in mining and insights into directions for future research, Int. J. Coal Geol. 179 (2017a) 28–44.
[3] O. Vardar, C. Zhang, I. Canbulat, B. Hebblewhite, A semi-quantitative coal burst risk classification system, Int. J. Min. Sci. Technol. 28 (5) (2018) 721–727.
[4] N. Cook, The basic mechanics of rockbursts, J. S. Afr. Inst. Min. Metall 64 (3) (1963) 71–81.
[5] N. Cook, E. Hoek, J. Pretorius, W. Ortlepp, M. Salamon, Rock mechanics applied to study of rockbursts, J. S. Afr. Inst. Min. Metall 66 (10) (1966) 436–528.
[6] N. Cook, C. Fenton, F. Lancaster, R. More-O'Ferall, W. Nienaber, A. van Schalkwijk, R. Steijn, J. Tyser, H. Wagner, D. Waterman, An Industry Guide to the Amelioration of Hazards of Rockbursts and Rockfalls, Chamber of Mines of South Africa, 1978.
[7] H. Maleki, J. Aggson, F. Miller, J. Agapito, Mine layout design for coal bump control, in: Proceedings 6th International Conference on Ground Control in Mining, West Virginia University, Morgantown, 1987, pp. 32–46.
[8] S. Spottiswoode, Volume excess shear stress and cumulative seismic moments, in: Proceedings 2nd International Symposium on Rockbursts and Seismicity in Mines, Pergamon, Minneapolis, 1990, p. A397.
[9] K.A. Heasley, An examination of energy calculations applied to coal bump prediction, in: Proceedings 32nd US Symposium on Rock Mechanics (USRMS), American Rock Mechanics Association, 1991.
[10] A. Jager, J. Ryder, A Handbook on Rock Engineering Practice for Tabular Hard Rock Mines, Safety in Mines Research Advisory Committee, Johannesburg: South Africa, 1999a.
[11] G.E. Blight, Soil mechanics principles in underground mining, J. Geotech. Eng. 110 (5) (1984) 567–581.
[12] J. Napier, Energy changes in a rockmass containing multiple discontinuities, J. S. Afr. Inst. Min. Metall 91 (5) (1991) 145–157.
[13] D.G.F. Hedley, Rockburst Handbook for Ontario Hardrock Mines, Canmet), 1992b.
[14] B.H. Brady, E.T. Brown, Rock Mechanics: for Underground Mining, Springer Science & Business Media, 2013.
[15] M. Salamon, Energy considerations in rock mechanics: fundamental results, J. S. Afr. Inst. Min. Metall 84 (8) (1984) 233–246.
[16] J. Ryder, Excess shear stress in the assessment of geologically hazardous situations, J. S. Afr. Inst. Min. Metall 88 (1) (1988) 27–39.
[17] C. Wei, C. Zhang, I. Canbulat, W. Huang, Numerical investigation into impacts of major fault on coal burst in longwall mining–A case study, Int. J. Rock Mech. Min. Sci. 147 (2021), 104907.
[18] R.J. Garvey, A Study of Unstable Rock Failures Using Finite Difference and Discrete Element Methods, Colorado School of Mines, 2013.
[19] E. Kias, Investigation of Unstable Failure in Underground Coal Mining Using the Discrete Element Method, PhD thesis, Colorado School of Mines, 2013.
[20] K.W. Harris, Improved Understanding of Coal Pillar Behavior and Bump Potential through the Ground Response Curve, 2015.
[21] R. Gu, Distinct Element Model Analyses of Unstable Failures in Underground Coal Mines, Colorado School of Mines, 2013.
[22] R. Gu, U. Ozbay, Distinct element analysis of unstable shear failure of rock discontinuities in underground mining conditions, Int. J. Rock Mech. Min. Sci. 68 (2014) 44–54.
[23] E.C. Poeck, Analyzing the Potential for Unstable Mine Failures with the Calculation of Released Energy in Numerical Models, Colorado School of Mines. Arthur Lakes Library, 2016.
[24] Z. Khademian, Computational Framework for Studying Seismicity Induced by Rock Engineering Activities, PhD thesis, Colorado School of Mines, 2018.
[25] Z. Khademian, U. Ozbay, Computational framework for simulating rock burst in shear and compression, Int. J. Rock Mech. Min. Sci. 110 (2018) 279–290.
[26] Z. Khademian, U. Ozbay, Modeling violent rock failures in tunneling and shaft boring based on energy balance calculations, Tunn. Undergr. Space Technol. 90 (2019) 62–75.
[27] F. Gao, L. Yang, Experimental and numerical investigation on the role of energy transition in strainbursts, Rock Mech. Rock Eng. 54 (9) (2021) 5057–5070.
[28] S.M.A. Manouchehrian, Numerical Modeling of Unstable Rock Failure, PhD thesis, Laurentian University of Sudbury, 2016.

[29] A. Manouchehrian, M. Cai, Analysis of rockburst in tunnels subjected to static and dynamic loads, J. Rock Mech. Geotech. Eng. 9 (6) (2017) 1031–1040.
[30] C. Zhang, I. Canbulat, F. Tahmasebinia, B. Hebblewhite, Assessment of energy release mechanisms contributing to coal burst, Int. J. Min. Sci. Technol. 27 (1) (2017b) 43–47.
[31] A. Manouchehrian, M. Cai, Numerical modeling of rockburst near fault zones in deep tunnels, Tunn. Undergr. Space Technol. 80 (2018) 164–180.
[32] O. Vardar, C. Wei, C. Zhang, I. Canbulat, Numerical investigation of impacts of geological faults on coal burst proneness during roadway excavation, Bull. Eng. Geol. Environ. 81 (1) (2022) 1–12.
[33] C. Wei, O. Vardar, C. Zhang, J. Watson, I. Canbulat, Numerical Analysis of Strain Energy Density at Development and Longwall Face, *2022 Resource Operators Conference*, Wollongong, Australia, 2022a.
[34] W. Ortlepp, T. Stacey, Rockburst mechanisms in tunnels and shafts, Tunn. Undergr. Space Technol. 9 (1) (1994) 59–65.
[35] W.D. Ortlepp, Rock Fracture and Rockbursts: an Illustrative Study, South African Institute of Mining and Metallurgy, Johannesburg, 1997.
[36] A. Jager, J. Ryder, A Handbook on Rock Engineering Practice for Tabular Hard Rock Mines, Safety in Mines Research Advisory Committee, Johannesburg, 1999b.
[37] J.M. Galvin, Ground Engineering Principles and Practices for Underground Coal Mining, Springer, 2016.
[38] A.T. Iannacchione, S.C. Tadolini, Occurrence, predication, and control of coal burst events in the US, Int. J. Min. Sci. Technol. 26 (1) (2016b) 39–46.
[39] S.J. Gibowicz, A. Kijko, An Introduction to Mining Seismology, Academic Press, 1994.
[40] A. Mendecki, G. Van Aswegen, P. Mountfort, *A Guide to Routine Seismic Monitoring in Mines*: Creda Communications, 1999 (Cape Town).
[41] B. Kostrov, Seismic moment and energy of earthquakes, and seismic flow of rock, Phys. Solid Earth 1 (1974) 23–44.
[42] K. Aki, P.G. Richards, Quantitative Seismology, University Science Books, 2002.
[43] Y. Potvin, J. Jarufe, J. Wesseloo, Interpretation of seismic data and numerical modelling of fault reactivation at El Teniente, Reservas Norte sector, Min. Technol. 119 (3) (2010) 175–181.
[44] G. Hofmann, L. Scheepers, Simulating fault slip areas of mining induced seismic tremors using static boundary element numerical modelling, Min. Technol. 120 (1) (2011) 53–64.
[45] J. Sjöberg, F. Perman, C. Quinteiro, L. Malmgren, C. Dahner-Lindkvist, M. Boskovic, Numerical analysis of alternative mining sequences to minimise potential for fault slip rockbursting, Min. Technol. 121 (4) (2012) 226–235.
[46] G. Hoffmann, S. Murphy, L. Scheepers, G. van Aswegen, Surface stress modelling of some shear slip seismic events that occurred in Anglogold Ashanti's tabular mines, in: Proceedings 8th International Symposium on Rockbursts and Seismicity in Mines, 2013, pp. 219–231.
[47] A. Sainoki, H.S. Mitri, Dynamic modelling of fault-slip with Barton's shear strength model, Int. J. Rock Mech. Min. Sci. 67 (2014) 155–163.
[48] A. Sainoki, H.S. Mitri, Effect of slip-weakening distance on selected seismic source parameters of mining-induced fault-slip, Int. J. Rock Mech. Min. Sci. 73 (2015) 115–122.
[49] L. Jiang, P. Kong, P. Zhang, J. Shu, Q. Wang, L. Chen, Q. Wu, Dynamic analysis of the rock burst potential of a longwall panel intersecting with a fault, Rock Mech. Rock Eng. 53 (2020) (2019) 1737–1754.
[50] C. Wei, C. Zhang, I. Canbulat, Numerical analysis of fault-slip behaviour in longwall mining using linear slip weakening law, Tunn. Undergr. Space Technol. 104 (2020), 103541.
[51] B. Hebblewhite, J. Galvin, A review of the geomechanics aspects of a double fatality coal burst at Austar Colliery in NSW, Australia in April 2014, Int. J. Min. Sci. Technol. 27 (1) (2017) 3–7.
[52] C. Wei, C. Zhang, I. Canbulat, A. Cao, L. Dou, Evaluation of current coal burst control techniques and development of a coal burst management framework, Tunn. Undergr. Space Technol. 81 (2018) 129–143.
[53] C. Wei, C. Zhang, I. Canbulat, Z. Song, L. Dai, A review of investigations on ground support requirements in coal burst-prone mines, Int. J. Coal Sci. Technol. 9 (1) (2022b) 1–20.
[54] D.G. Hedley, Rockburst Handbook for Ontario Hardrock Mines, Canmet, 1992a.
[55] Itasca, Universal Distinct Element Code v6.00 Users' Manual, Itasca, Minneapolis), 2014.
[56] A. McGarr, S. Spottiswoode, N. Gay, W. Ortlepp, Observations relevant to seismic driving stress, stress drop, and efficiency, J. Geophys. Res. Solid Earth 84 (B5) (1979) 2251–2261.
[57] S. Spottiswoode, Seismic attenuation in deep-level mines, Rockbursts and Seismicity in Mines, 1993, pp. 409–414.